MNRAS **497,** 1563–1570 (2020)
Advance Access publication 2020 July 10

doi:10.1093/mnras/staa2018

Dynamics of black hole–neutron star binaries in young star clusters

Sara Rastello [1,2]★ Michela Mapelli [1,2,3]★ Ugo N. Di Carlo [2,3,4] Nicola Giacobbo [1,2,3]★ Filippo Santoliquido,[1,2] Mario Spera [1,2,5,6] Alessandro Ballone [1,2] and Giuliano Iorio [1,2]

[1]*Physics and Astronomy Department Galileo Galilei, University of Padova, Vicolo dell'Osservatorio 3, I-35122 Padova, Italy*
[2]*INFN-Padova, Via Marzolo 8, I–35131 Padova, Italy*
[3]*INAF-Osservatorio Astronomico di Padova, Vicolo dell'Osservatorio 5, I-35122 Padova, Italy*
[4]*Dipartimento di Scienza e Alta Tecnologia, University of Insubria, Via Valleggio 11, I-22100 Como, Italy*
[5]*Center for Interdisciplinary Exploration and Research in Astrophysics (CIERA), Evanston, IL 60208, USA*
[6]*Department of Physics and Astronomy, Northwestern University, Evanston, IL 60208, USA*

Accepted 2020 July 4. Received 2020 June 30; in original form 2020 April 24

ABSTRACT

Young star clusters are likely the most common birthplace of massive stars across cosmic time and influence the formation of compact binaries in several ways. Here, we simulate the formation of black hole–neutron star binaries (BHNSs) in young star clusters, by means of the binary population synthesis code MOBSE interfaced with the *N*-body code NBODY6++GPU. BHNSs formed in young star clusters (dynamical BHNSs) are significantly more massive than BHNSs formed from isolated binaries (isolated BHNSs): ∼40 per cent of the dynamical BHNS mergers have a total mass of >15 M$_\odot$, while only ∼0.01 per cent of the isolated BHNS mergers have mass in excess of this value. Hence, our models strongly support a dynamical formation scenario for GW190814, given its total mass of ∼26 M$_\odot$, if this event is a BHNS merger. All our dynamical BHNSs are ejected from their parent star cluster before they reach coalescence. Thus, a significant fraction of BHNS mergers occurring in the field might have originated in a young star cluster. The mass spectrum of BHNS mergers from gravitational-wave detections will provide a clue to differentiate between dynamical and isolated formation of BHNSs.

Key words: black hole physics – gravitational waves – stars: black holes – stars: kinematics and dynamics – stars: neutron – galaxy: open clusters and associations: general.

1 INTRODUCTION

The LIGO–Virgo collaboration (LVC) has detected three binary black hole (BBH) mergers during the first observing run (O1; Abbott et al. 2016a,b,c) and eight additional gravitational-wave (GW) events during the second observing run (O2), seven of them interpreted as BBHs and one associated with a binary neutron star (BNS; Abbott et al. 2017a,b,c, 2019). The third observing run (O3) has just ended and already led to the publication of GW190425 (Abbott et al. 2020a), a compact binary coalescence with a total mass of ∼3.4 M$_\odot$. This is likely the second observed BNS merger, but has total mass significantly larger than the known Galactic BNSs (Özel & Freire 2016). No black hole–neutron star (BHNS) mergers were observed in O1 and O2 (Abbott et al. 2019; Wei & Feng 2019), and we do not know any black hole (BH)–pulsar binary from radio observations. While we were addressing reviewer's comments, the LVC published GW190814 (Abbott et al. 2020b), a compact binary merger with a primary mass of $m_1 = 23.2^{+1.1}_{-1.0}$ M$_\odot$ and a secondary mass of $m_2 = 2.59^{+0.08}_{-0.09}$ M$_\odot$. The secondary object might be either the lowest mass BH or the most massive NS known to date. In the latter case, GW190814 would be the first BHNS ever observed.

BHNSs have attracted considerable interest. The observation of a tight BH–pulsar binary would be a holy grail of gravity, and is one of the main scientific goals of the Square Kilometer Array (SKA).[1] The lack of observations of BH–pulsar binaries with current radio facilities is not surprising: Pfahl, Podsiadlowski & Rappaport (2005) estimate that there are no more than one BH–recycled pulsar binary in the Milky Way for every 100–1000 BNSs, of which 15 are currently known (Tauris et al. 2017; Farrow, Zhu & Thrane 2019).

Similar to BNSs, BHNS mergers might lead to the emission of short gamma-ray bursts under some circumstances (Blinnikov et al. 1984; Eichler et al. 1989; Narayan, Piran & Shemi 1991; Paczynski 1991; Mao, Narayan & Piran 1994; Bethe & Brown 1998, 1999; Fryer, Woosley & Hartmann 1999; Popham, Woosley & Fryer 1999; Ruffert & Janka 1999; Zappa et al. 2019). The properties of possible optical/near-infrared counterparts to BHNSs are still a matter of debate (e.g. Fernández et al. 2017; Barbieri et al. 2019; Andreoni et al. 2020).

From the non-detection of BHNS mergers in O1 and O2, the LVC inferred an upper limit of ∼610 Gpc^{-3} yr^{-1} for the local merger rate density of BHNSs (Abbott et al. 2019). Theoretical predictions for the BHNS local merger rate density $\mathcal{R}_{\rm BHNS}$ come mostly from the isolated binary scenario: Dominik et al. (2015) predict $\mathcal{R}_{\rm BHNS} \sim$ 0.04–20 Gpc^{-3} yr^{-1}, consistent with earlier theoretical predictions (Sipior & Sigurdsson 2002; Pfahl et al. 2005; Belczynski et al. 2007, 2010; O'Shaughnessy, Kalogera & Belczynski 2010). Based on the

★ E-mail: sara.rastello88@gmail.com (SR); michela.mapelli@inaf.it (MM); giacobbo.nicola@gmail.com (NG)

[1]https://www.skatelescope.org/

coupling between population-synthesis simulations and cosmological simulations, Mapelli & Giacobbo (2018) find $\mathcal{R}_{\rm BHNS} \sim 10$–$100$ Gpc^{-3} yr^{-1}, consistent with Artale et al. (2019) ($\mathcal{R}_{\rm BHNS} \sim 60$ Gpc^{-3} yr^{-1}). Finally, recent population-synthesis models combined with a data-driven approach yield $\mathcal{R}_{\rm BHNS} \sim 4$–$350$ Gpc^{-3} yr^{-1} (Baibhav et al. 2019; Giacobbo & Mapelli 2020; Tang et al. 2020).

Less attention has been paid to the dynamical formation of BHNSs in dense stellar systems, such as globular clusters or young star clusters (YSCs). We have known for a long time that dynamical exchanges are likely to occur when the mass of the intruder is larger than the mass of one of the two components of the binary system (Hills & Fullerton 1980; Sigurdsson & Hernquist 1993; Sigurdsson & Phinney 1995). Since BHs and their stellar progenitors are among the most massive objects in a star cluster, we expect them to be very efficient in acquiring companions through dynamical exchanges, unless they are ejected earlier from the stellar system. Previous studies have shown that dynamical exchanges significantly contribute to the formation of BBHs in globular clusters (e.g. Portegies Zwart & McMillan 2000; Rodriguez et al. 2015; Rodriguez, Chatterjee & Rasio 2016; Fragione & Kocsis 2018; Hong et al. 2018; Rodriguez et al. 2018, 2019; Samsing 2018; Arca Sedda & Mastrobuono-Battisti 2019; Choksi et al. 2019; Samsing, Hamers & Tyles 2019; Kremer et al. 2020), YSCs (e.g. Ziosi et al. 2014; Mapelli 2016; Fujii, Tanikawa & Makino 2017; Di Carlo et al. 2019a,b), and open star clusters (e.g. Banerjee, Baumgardt & Kroupa 2010; Tanikawa 2013; Banerjee 2017, 2018; Banerjee et al. 2019; Kumamoto, Fujii & Tanikawa 2019, 2020; Rastello et al. 2019).

Clausen, Sigurdsson & Chernoff (2013) studied the dynamical formation of BHNSs in globular clusters (see also Devecchi et al. 2007; Clausen, Sigurdsson & Chernoff 2014), finding a local merger rate density of $\sim$0.01–0.17 Gpc^{-3} yr^{-1}. While BHNSs actively form by exchange in globular clusters, most of these systems merge in the first $\sim$4 Gyr and are subsequently ejected; hence (considering that most globular clusters formed 12 Gyr ago), they cannot be detected by LIGO and Virgo. Similarly, Ye et al. (2020) find a local BHNS merger rate of $\mathcal{R}_{\rm BHNS} \sim 0.009$–$0.06$ Gpc^{-3} yr^{-1} ($\mathcal{R}_{\rm BHNS} \sim 5.5$ Gpc^{-3} yr^{-1} in their extremely optimistic model) from globular clusters. Fragione & Loeb (2019a,b) studied BHNS mergers originated in triple systems deriving $\mathcal{R}_{\rm BHNS} \sim 1.9 \times 10^{-4}$–$22$ Gpc^{-3} yr^{-1}. Finally, Ziosi et al. (2014) estimate an upper limit for the local merger rate of BHNSs from YSCs ($\mathcal{R}_{\rm BHNS} \leq 100$ Gpc^{-3} yr^{-1}). The contribution of YSCs to the local merger rate of BHNSs might be significantly higher than that of globular clusters, because the latter formed only in the early Universe, while the former continuously form across cosmic history.

BHNS mergers from isolated binary evolution appear to have a relatively high mass ratio ($q_{\rm BHNS} = m_{\rm NS}/m_{\rm BH} \sim 0.2$–$0.3$; Giacobbo & Mapelli 2018; Mapelli & Giacobbo 2018; Mapelli et al. 2019): The mass of the BH is generally $m_{\rm BH} \leq 12$ M$_\odot$, while the mass of the NS tends to be higher than that of Galactic BNSs ($m_{\rm NS} \sim 1.5$–2 M$_\odot$). We found no estimates of the mass distribution of BHNSs from dynamical simulations in the literature: Clausen et al. (2013) just study two test cases in which the mass of the BH is 7 and 35 M$_\odot$, respectively.

Here, we study the formation and evolution of BHNSs in YSCs. YSCs are the nursery of massive stars (which are thought to be the progenitors of BHs and NSs). Thus, it is reasonable to expect that compact objects participate in the dynamics of their parent YSCs, at least for few Myr. Note that the dynamical evolution of globular clusters and YSCs is significantly different. Globular clusters have a two-body relaxation time-scale $t_{\rm rlx}$ of several hundreds of Myr (Spitzer 1987) and a central escape velocity of $\sim$30 km s^{-1}, while YSCs have $t_{\rm rlx} \sim 10$–100 Myr and a central escape velocity of a few km s^{-1}. Hence, while a BH can undergo a long chain of exchanges in a globular cluster, before being ejected by dynamical or relativistic kicks, usually the time of ejection from a YSC is much shorter ($\sim$ few Myr). Moreover, the core-collapse time-scale in a YSC is $\leq$ few Myr (Mapelli & Bressan 2013). This implies that most exchanges in globular clusters involve BHs and neutron stars (NSs) that have already formed, while most interactions in YSCs happen when the progenitor stars have not yet collapsed to a BH or NS, with significant differences in the binary compact object populations (Di Carlo et al. 2019b; Kumamoto et al. 2019). Furthermore, while globular clusters formed only in the early epochs ($\sim$8–13 Gyr ago), YSCs represent the main formation pathway of massive stars down to the local Universe (Lada & Lada 2003; Portegies Zwart, McMillan & Gieles 2010).

Simulating YSCs requires challenging N-body simulations, coupled with binary population-synthesis calculations. Here, we discuss a new set of 100 002 direct N-body simulations of YSCs, including a high binary fraction ($f_{\rm b} = 0.4$) and fractal initial conditions. We adopted the code NBODY6++GPU (Wang et al. 2015, 2016), coupled with the binary population-synthesis code MOBSE (Giacobbo, Mapelli & Spera 2018), as described in Di Carlo et al. (2019b).

2 METHODS

The simulations discussed in this paper were performed with the same code as described in Di Carlo et al. (2019b). In particular, we use the direct summation N-body code NBODY6++GPU (Wang et al. 2015) coupled with the population-synthesis code MOBSE (Mapelli et al. 2017; Giacobbo & Mapelli 2018, 2019; Giacobbo et al. 2018). MOBSE is an upgrade of BSE (Hurley, Tout & Pols 2002), including up-to-date prescriptions for stellar winds, for the outcome of core-collapse supernovae (SNe) and for pair instability and pulsational pair instability. Mass-loss by stellar winds is described as $\dot{M} \propto Z^{\beta}$ for all massive hot stars (O-type, B-type, Wolf–Rayet, and luminous blue variable stars). The index β is defined as $\beta = 0.85$ if $\Gamma_{\rm e} < 2/3$, $\beta = 2.45 - \Gamma_{\rm e}$ 2.4 if $2/3 \leq \Gamma_{\rm e} \leq 1$, and $\beta = 0.05$ if $\Gamma_{\rm e} > 1$ (see Giacobbo et al. 2018, for details).

Core-collapse SNe are described as in Fryer et al. (2012). In particular, here we adopt the rapid core-collapse SN model, which suppresses the formation of compact objects with mass in the 2–5 M$_\odot$ range. According to this model, stars developing a carbon–oxygen core $m_{\rm CO} \gtrsim 11$ M$_\odot$ collapse to a BH directly. Finally, pair instability and pulsational pair instability are modelled as described in Spera & Mapelli (2017) and Mapelli et al. (2020). This implementation produces a mass gap in the BH mass spectrum between $m_{\rm BH} \sim 65$ and 120 M$_\odot$.

We model YSCs with three different metallicities: $Z = 0.02$, 0.002, and 0.0002. We ran 33 334 N-body simulations per each metallicity for a total of 100 002 simulations.

YSC masses are sampled in the range $300 \leq M_{\rm SC}/{\rm M}_\odot < 1000$ from a distribution ${\rm d}N/{\rm d}M_{\rm SC} \propto M_{\rm SC}^{-2}$, reminiscent of the distribution of YSCs in the Milky Way (Lada & Lada 2003). Hence, in this work we focus on the smallest star clusters. We will consider more massive star clusters in a follow-up work. We choose the initial star cluster half-mass radius $r_{\rm h}$ according to the Marks and Kroupa relation (Marks et al. 2012), which relates the total mass $M_{\rm SC}$ of an SC at birth with its initial half-mass radius $r_{\rm h}$:

$$r_{\rm h} = 0.10^{+0.07}_{-0.04}\,{\rm pc}\left(\frac{M_{\rm SC}}{{\rm M}_\odot}\right)^{0.13\pm0.04}. \quad (1)$$

We generate models of star clusters that are characterized by fractal substructures (as described in Goodwin & Whitworth 2004), by using the software MCLUSTER (Küpper et al. 2011). The fractal dimension

Table 1. Initial conditions.

Set	Run number	M_{SC} ($M_\odot$)	r_h (pc)	r_t (pc)	Z	f_{bin}	D	IMF	m_{min} ($M_\odot$)	m_{max} ($M_\odot$)
Z0002	33334	3×10^2–10^3	$0.1 \times (M_{SC}/M_\odot)^{0.13}$	9.9–13.9	0.0002	0.4	1.6	Kroupa (2001)	0.1	150
Z002	33334	3×10^2–10^3	$0.1 \times (M_{SC}/M_\odot)^{0.13}$	9.9–13.9	0.002	0.4	1.6	Kroupa (2001)	0.1	150
Z02	33334	3×10^2–10^3	$0.1 \times (M_{SC}/M_\odot)^{0.13}$	9.9–13.9	0.02	0.4	1.6	Kroupa (2001)	0.1	150

Note. Column 1: Name of the simulation set; column 2: number of runs; column 3: total mass of YSCs (M_{SC}); column 4: half-mass radius (r_h); column 5: tidal radius (r_t); column 6: metallicity (Z); column 7: initial binary fraction (f_{bin}); column 8: fractal dimension (D); column 9: IMF; column 10: minimum mass of stars (m_{min}); column 11: maximum mass of stars (m_{max}).

D is set to be 1.6. We choose fractal initial conditions, because observations (Sánchez & Alfaro 2009; Küpper et al. 2011; Kuhn et al. 2019) and hydrodynamical simulations (Ballone et al. 2020) indicate that embedded star clusters have a small fractal dimension. The YSCs are initialized in virial equilibrium (with $T/|V| = 0.5$).

Star masses are extracted from a Kroupa (Kroupa 2001) initial mass function (IMF) with $0.1 < M < 150$ $M_\odot$. We did not assume any relation between star cluster mass and maximum stellar mass.[2] The orbital parameters of binary systems are generated following the distributions by Sana et al. (2012). In particular, binary eccentricities e are randomly drawn from a distribution $\mathcal{P}(e) \propto e^{-0.42}$ with $0 \leq e < 1$, while orbital periods P are randomly selected from $\mathcal{P}(\Pi) \propto \Pi^{-0.55}$, where $\Pi = \log_{10}(P/\mathrm{days})$ and $0.15 \leq \Pi \leq 6.7$. We assume an initial total binary fraction $f_{bin} = 0.4$. MCLUSTER assigns the companion stars based on mass: Stars are randomly paired by enforcing a distribution $\mathcal{P}(q) \propto q^{-0.1}$, where $q = m_2/m_1$ is the ratio of the mass of the secondary to the mass of the primary star, consistent with Sana et al. (2012). All the stars more massive than 5 $M_\odot$ are forced to be members of binary systems, while stars with masses of <5 $M_\odot$ are randomly paired only till we reach a total binary fraction $f_{bin} = 0.4$. The result of this procedure is that the most massive stars (down to 5 $M_\odot$ in our case) are all members of a binary system, while the binary fraction drops to lower values for lower star masses. This is consistent with observational results (e.g. Moe & Di Stefano 2017).

The force integration in NBODY6++GPU includes a solar neighbourhood-like static external tidal field. In particular, the potential is point-like and the simulated star clusters are assumed to be on a circular orbit around the centre of the Milky Way with a semimajor axis of 8 kpc (Wang et al. 2016). We integrate each YSC until its dissolution or for a maximum time $t = 100$ Myr. Initially, all YSCs are tidally underfilling. As time passes, the clusters expand and the smallest ones (in the mass range 300–700 $M_\odot$) become tidally overfilling. Only the most massive systems ($700 < M_{SC}/M_\odot < 1000$) remain tidally underfilling for the entire simulation. Our choice of the tidal field might affect the merger rate: YSCs closer to (farther away from) the Galactic Centre feel stronger (weaker) tidal forces, reducing (increasing) their dissolution time-scale. We will explore the effect of different tidal fields in future works.

At a time $t > 100$ Myr, the BHNSs that escaped[3] from the cluster evolve only due to the emission of gravitational radiation. We estimate the coalescence time-scale of these binaries with the formalism described in Peters (1964).

[2]Weidner & Kroupa (2006) and Weidner, Kroupa & Bonnell (2010) claim the existence of a relation between star cluster mass and maximum stellar mass. If we had included such relation in our initial conditions, we would have prevented the formation of the most massive stars in the smallest cluster, possibly slowing down the dissolution of these clusters.

[3]We define escapers as those stars and binaries that reach a distance from the centre of the YSC larger than twice the tidal radius of the cluster, as calculated by NBODY6++GPU (Aarseth 2012).

A summary of the initial conditions of the simulations is reported in Table 1.

The main differences of our simulations with respect to the ones of Di Carlo et al. (2019b) are (i) the mass range of star clusters [we simulate star clusters from 300 to 1000 $M_\odot$, while the mass range in Di Carlo et al. (2019b) is (1–3) $\times$ 10^4 $M_\odot$], (ii) the metallicity range (Di Carlo et al. 2019b consider only $Z = 0.002$, while we also simulate $Z = 0.0002$ and 0.02), (iii) the treatment of common envelope (whose parameter α was set to 3 by Di Carlo et al. 2019b, while here we adopt $\alpha = 5$, consistent with Fragos et al. 2019), (iv) the choice of the prescription for core-collapse SNe (here we choose the rapid model by Fryer et al. 2012, while Di Carlo et al. 2019b assumed the delayed model and have BHs with masses down to $\sim$3 $M_\odot$), and (v) the SN kick model: in Di Carlo et al. (2019b), we assumed the same model as Fryer et al. (2012), while here we use the same prescriptions as run CC15α15 in Giacobbo & Mapelli (2018). In particular, we assume that NSs receive a natal kick randomly drawn from a Maxwellian with a one-dimensional root mean square σ =15 km s^{-1}. BH kicks are drawn as $v_{BH} = (1 - f_{fb})\, v_{NS}$, where v_{NS} is the NS kick drawn as described above and f_{fb} is the fallback fraction defined in Fryer et al. (2012).

In addition, we simulate a comparison sample of isolated binaries with the stand-alone version of MOBSE. The isolated binary sample is composed of 3×10^7 binary systems (10^7 for each metallicity). The isolated sample is the same as run CC15α5 in Giacobbo & Mapelli (2018).

3 RESULTS

3.1 Population of BHNSs formed in YSCs

Fig. 1 shows the population of BHNSs formed in our N-body simulations at $t = 100$ Myr. This sample includes both systems that merge within a Hubble time and systems with larger orbital separation.

The BHNSs that form from the same binary star (i.e. the stellar progenitors of the BH and the NS were already bound in the initial conditions) are labelled as 'original BHNSs'. The BHNSs that form through dynamical exchanges are labelled as 'exchanged BHNSs'. We also consider a comparison sample of 'isolated BHNSs', which form in the field from isolated binary evolution. It is important to note that dynamics affects not only exchanged binaries (which, indeed, form by dynamical encounters), but even original binaries: Close dynamical encounters shrink (or widen) the semimajor axis of a binary star, change its orbital eccentricity, and can even unbind the binary. In particular, lighter and wider binaries (soft binaries) tend to be widened/ionized, while massive and tight binaries (hard binaries) tend to increase their binding energy and shrink (Heggie 1975).

Fig. 1 shows that the percentage of exchanged binaries increases with the total mass of the star cluster, at all considered metallicities. The percentage of exchanged binaries is higher in metal-poor star

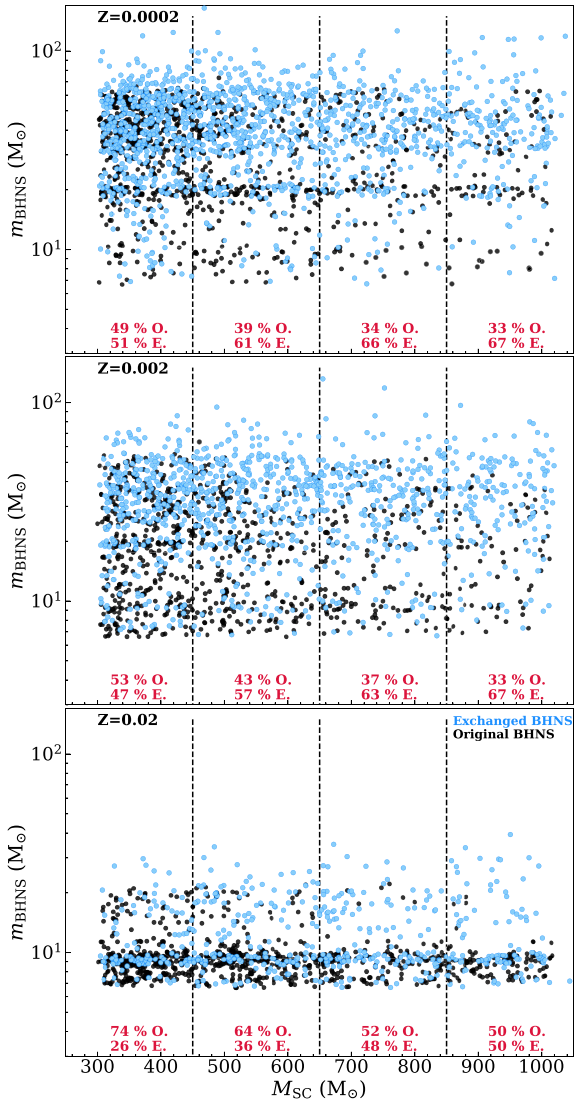

Figure 1. Distribution of BHNS total mass versus YSC mass for $Z = 0.0002$, 0.002, and 0.02 (top, middle, and bottom panels, respectively) at $t = 100$ Myr. Black circles: original BHNSs; blue circles: exchanged BHNSs. Each scatter plot is divided into four bins of cluster mass in the range: $250 < M_{\rm SC}/M_\odot < 450$, $450 < M_{\rm SC}/M_\odot < 650$, $650 < M_{\rm SC}/M_\odot < 850$, and $850 < M_{\rm SC}/M_\odot < 1050$. The percentage of exchanged (E) and original (O) BHNSs in each mass range is indicated in the bottom part of each bin.

clusters (from ∼50 to ∼70 per cent at $Z = 0.0002$–0.002, depending on the mass of the cluster) than that in metal-rich ones (from ∼30 to ∼50 per cent at solar metallicity, also depending on the mass of the cluster).

These findings can be interpreted as a result of the interplay between stellar evolution and dynamics. According to our assumptions (in particular, to the Marks et al. 2012 relation), our more massive star clusters are denser than the smaller ones; hence, dynamical encounters and exchanges are more common in the former than in the latter. Moreover, BHs are generally more massive in metal-poor clusters; hence, BHs born in metal-poor star clusters are more efficient in acquiring companions through exchanges than BHs in metal-rich clusters.

From Fig. 1, we also note that exchanged binaries are generally more massive than original BHNSs. Dynamics leads to the formation

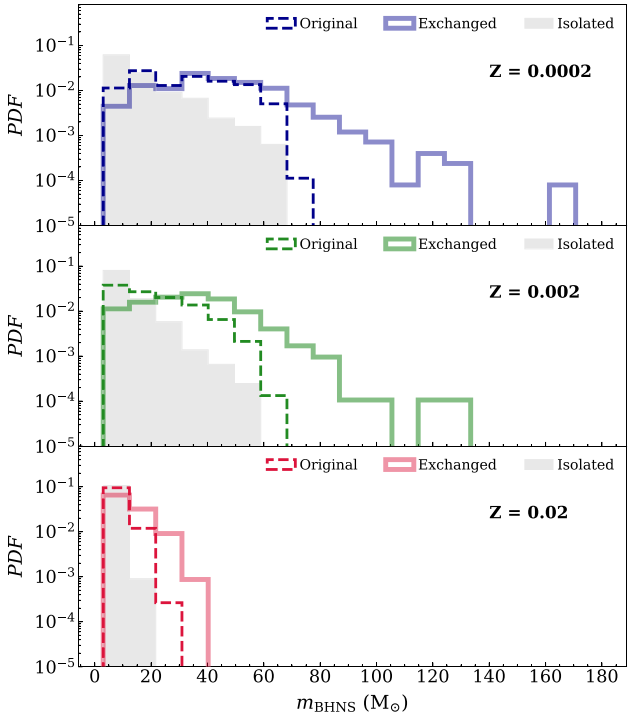

Figure 2. Mass of BHNSs ($m_{\rm BHNS}$) formed in YSCs and in isolation. The panels from top to bottom refer to $Z = 0.0002$ (blue), 0.002 (green), and 0.02 (red), respectively. The filled grey histograms refer to isolated binaries. Solid lines: exchanged BHNSs; dashed lines: original BHNSs.

of more massive binaries because it allows the formation of very massive BHs through multiple stellar collisions and dynamical exchanges allow such massive BHs to pair with other compact objects.

Moreover, we find no evidence of correlation between the mass of the parent YSC and the mass of the BHNSs. This is true for both original and exchanged binaries. Each of the four bins of cluster mass shows very similar BHNS mass distributions. The large number of BHNSs in low-mass clusters is a direct effect of the cluster mass distribution we adopted ($dN/dM_{\rm SC} \propto M_{\rm SC}^{-2}$), because of which we simulated many more low-mass YSCs than high-mass YSCs. To investigate any correlation between YSC mass and the number of BHNSs, we define the efficiency of BHNS formation per cluster mass as $\eta_f(M_{\rm SC}) = \mathcal{N}_{\rm BHNS}(M_{\rm SC})/M_*(M_{\rm SC})$, where $\mathcal{N}_{\rm BHNS}(M_{\rm SC})$ is the total number of BHNSs formed in YSCs with a mass of $M_{\rm SC}$ and $M_*(M_{\rm SC})$ is the total initial stellar mass locked in the simulated YSCs with a mass of $M_{\rm SC}$. Grouping our YSCs in four mass bins (the same as in Fig. 1), we find that $\eta_{\rm f} = (7 \times 10^{-5})$–$(1.6 \times 10^{-4})$ $M_\odot^{-1}$, varying only by a factor of 2 in the considered YSC mass range.

3.2 YSCs versus isolated binaries

Fig. 2 compares the mass distribution of BHNSs formed in YSCs with that of BHNSs formed in isolation. The maximum mass of a BHNS, $m_{\rm BHNS,\,max}$, is similar in original and isolated BHNSs. Its value is ∼73, ∼63, and ∼22 $M_\odot$ at $Z = 0.0002$, 0.002, and 0.02, respectively. In contrast, the maximum BHNS mass is significantly larger in the case of exchanged BHNSs: ∼164, ∼131, and ∼39 $M_\odot$ at $Z = 0.0002$, 0.002, and 0.02, respectively.

The main reason of this striking difference between exchanged binaries and the other systems is that BHs in YSCs can form from

the merger of two (or more) stars (Portegies Zwart et al. 2004). In this case, the mass of the BH can be significantly higher than the mass of a BH formed from a single star and can even be in the pair-instability mass gap (see e.g. Di Carlo et al. 2019a, for details). Such massive BHs are alone at birth, but they can acquire a companion through dynamical exchanges if they are members of a star cluster.

Another crucial difference between isolated BHNSs and dynamical BHNSs is the number of light systems ($m_{\rm BHNS} \lesssim 15$ M$_\odot$) and (as a consequence) the slope of the entire mass function. Light BHs are the most common ones in isolated BHNSs, while their contribution is significantly smaller in dynamical (both exchanged and original) BHNSs, especially at low Z. This is an effect of dynamics, because dynamical exchanges tend to suppress the lightest binaries. Soft[4] BHNSs and their soft progenitor binary stars tend to be disrupted by dynamical encounters during YSC evolution. Less than 5 per cent of such soft binaries survive till the end of the simulation.

About 96 per cent of all the BHNSs formed in YSCs have been ejected from the stellar system by the end of the simulations (100 Myr). As the metallicity of the systems increases, the percentage of retained BHNSs decreases: 5 per cent at $Z = 0.0002$, 4 per cent at $Z = 0.002$, and <1 per cent at $Z = 0.02$. This difference is expected, because BHNSs are generally more massive at low metallicity and thus can be more easily retained inside the YSC. About 60 per cent of the ejected BHNSs are kicked off the YSC through dynamical encounters, while the remaining 40 per cent have escaped because of the SN kicks. All the ejected BHNSs escape before cluster's dissolution.

3.3 Coalescence of BHNSs from YSCs and from isolated binaries

In this section, we focus on BHNSs that reach coalescence within a Hubble time by emission of GWs. In our dynamical simulations, we find 69 BHNS mergers, of which 31, 36, and 2 are at metallicity $Z = 0.0002$, 0.002, and 0.02, respectively. Fig. 3 shows the mass of the NS ($m_{\rm NS}$) versus the mass of the BH ($m_{\rm BH}$) of BHNS mergers. The majority of coalescing BHNSs from YSCs are original binaries (84 per cent), while the remaining (16 per cent) are exchanged binaries. The three most massive BHs ($m_{\rm BH} > 40$ M$_\odot$) in coalescing BHNSs are exchanged systems, but even original BHNSs can host significantly massive BHs. We estimate that 40 per cent of the BHNS mergers have a BH component with a mass of $m_{\rm BH} > 15$ M$_\odot$. 78 per cent of such massive merging BHNSs are original, while 22 per cent are exchanged binaries. 49 per cent of the massive merging BHNSs form at $Z = 0.0002$ and 51 per cent at $Z = 0.002$. We find no massive BHNS mergers at solar metallicity.

The mass of the NS component of BHNS mergers is always in the range $1.1 \leq m_{\rm NS}/{\rm M}_\odot \leq 2$, but this is a consequence of the assumed prescription for core-collapse SNe: No compact objects can form with mass 2–5 M$_\odot$ according to the rapid core-collapse SN model by Fryer et al. (2012). If we had used the delayed core-collapse SN model by the same authors, we would likely have found compact-object masses in the 2–5 M$_\odot$ range.

Fig. 4 shows the cumulative distribution of total mass, chirp mass $\mathcal{M}_{\rm BHNS}$, and mass ratio $q_{\rm BHNS} = m_{\rm NS}/m_{\rm BH}$ of BHNS mergers. The mass ratios are always <0.4, consistent with previous results (e.g. Giacobbo & Mapelli 2018). Dynamical and isolated BHNS mergers have a similar minimum mass ratio of $q_{\rm min} \sim 0.02$, but small mass ratios ($q < 0.15$) are significantly more common in dynamical BHNSs than in isolated BHNSs.

[4]A soft binary star is a binary star with binding energy smaller than the average kinetic energy of a star in the cluster (Heggie 1975).

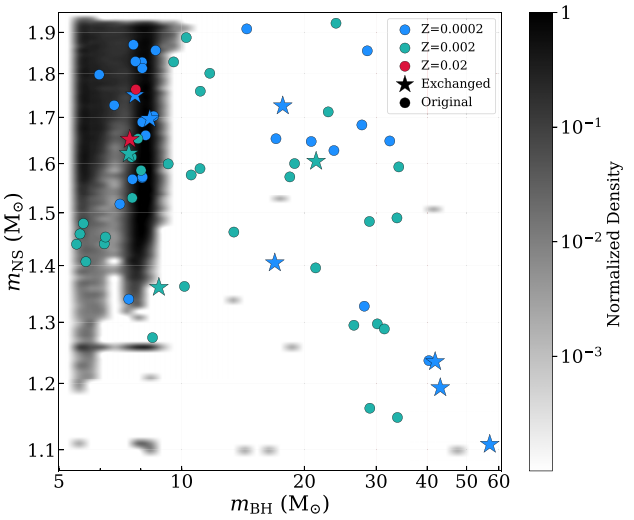

Figure 3. Mass of the BH ($m_{\rm BH}$) versus mass of the NS ($m_{\rm NS}$) of BHNS mergers. Circles: original BHNSs; stars: exchanged BHNSs. Blue: $Z = 0.0002$; green: $Z = 0.002$; red: $Z = 0.02$. Filled contours (grey colour map) indicate isolated BHNS mergers (Giacobbo et al. 2018) for all the three metallicities.

The chirp masses of dynamical BHNS mergers have a much broader range of values than the isolated systems: The former extend from $\mathcal{M}_{\rm BHNS} \sim 2.7$ to 5.4 M$_\odot$ (with negligible differences between original and exchanged BHNSs), while the latter are more concentrated in the $2 \leq \mathcal{M}_{\rm BHNS}/{\rm M}_\odot \leq 4$ range with a tail at higher chirp mass.

In summary, massive BH components ($m_{\rm BH} > 15$ M$_\odot$) are significantly more common in dynamical BHNS mergers than in isolated BHNS mergers. Massive BHs are very common not only in exchanged BHNSs, but even in original BHNSs. This result is easy to understand in the case of exchanged BHNSs (these can host more massive BHs born from single star evolution or from previous stellar mergers), but is trickier to grasp for original BHNSs. The higher fraction of massive BHs in original BHNSs with respect to isolated BHNSs comes from an interplay between binary evolution and dynamics. As we have already discussed in Giacobbo & Mapelli (2018), the most massive BHs in our models come from metal-poor stars with masses of ∼60–80 M$_\odot$. These stars develop very large radii (hundreds to thousands of solar radii; Spera et al. 2019) during their giant phase. If the initial orbital separation of the binary star was smaller than these large radii, the binary star merges before giving birth to a BHNS. For larger orbital separation, the binary star undergoes Roche lobe overflow, which tends to equalize the final mass of the two compact objects: The final BHNS might merge by GW emission, but the mass of the BH is significantly smaller than that expected from single star evolution because of mass transfer and envelope removal. Finally, if the binary is too large to undergo Roche lobe overflow (orbital separation $a \gtrsim 10^3$ R$_\odot$; Spera et al. 2019), the mass of the BH in the final BHNS is the same as expected from single star evolution (i.e. 50–65 M$_\odot$ for a metal-poor progenitor with zero-age main-sequence mass ∼60–80 M$_\odot$), but, if the binary is isolated, the final orbital separation is too large to lead to coalescence by GW emission. In a dynamical environment such as a YSC, such original BHNSs with a massive BH component can shrink by dynamical encounters and might be able to merge by GW emission.

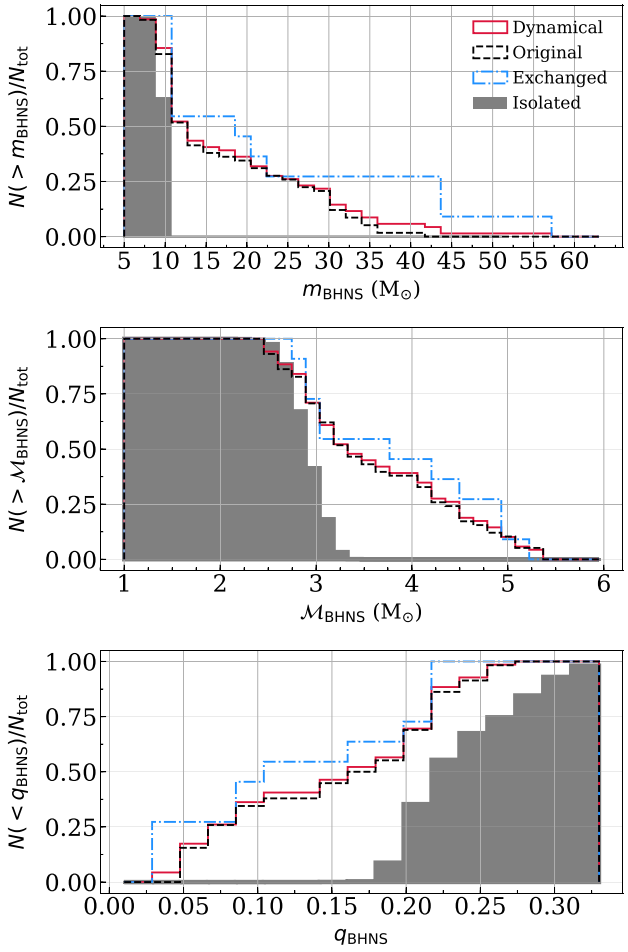

Figure 4. Cumulative distribution of total mass $m_{\rm BHNS}$ (top), chirp mass $\mathcal{M}_{\rm BHNS}$ (middle), and mass ratio $q_{\rm BHNS}$ (bottom) of the simulated BHNS mergers in YSCs and in isolation. Each line is normalized to the total number of mergers belonging to that specific class. Solid red line: all dynamical BHNS mergers (both exchanged and original BHNS mergers); dashed black line: original BHNS mergers; dot–dashed blue line: exchanged BHNS mergers; grey filled histograms: isolated BHNS mergers. The three metallicities are displayed together.

Finally, all the dynamical BHNS mergers happen after the binary was ejected from the YSC. About 70 per cent of them are ejected via dynamical encounters, while the remaining ∼30 per cent are kicked off by SN kicks.

This is a crucial result because it means that the vast majority of BHNSs born in YSCs are field binaries by the time of their merger. The population of BHNS mergers in the field is then the result of a mixture between genuine isolated binaries and dynamical systems previously ejected from their parent star cluster.

3.4 Merger efficiency and rate

We estimate the merger efficiency, $\eta(Z)$, defined as the number of mergers $\mathcal{N}_{\rm TOT}(Z)$ within a Hubble time, divided by the total initial stellar mass of the YSCs at a given metallicity: $\eta(Z) = \mathcal{N}_{\rm TOT}(Z)/M_*(Z)$, where $M_*(Z) = \sum_i M_{{\rm SC},i}(Z)$. The merger efficiency is a good proxy for the merger rate, because it does not depend on assumptions on star formation rate, metallicity evolution, and delay time (apart from its integrated value). Table 2 shows the merger efficiency for BHNSs from YSCs ($\eta_{\rm YSC}$) and from isolated binaries ($\eta_{\rm IB}$) at different metallicities. In metal-poor systems ($Z = 0.0002$ and 0.002), the merger efficiency of BHNSs from small YSCs is about a factor of 10 lower than the BHNS merger efficiency from isolated binaries. In contrast, at solar metallicity ($Z = 0.02$) the BHNS merger efficiency associated with YSCs is about a factor of 40 higher than the BHNS merger efficiency from isolated binaries.

Table 2. Merger efficiency of BHNSs from YSCs and from isolated binaries. Column 1: metallicity Z; column 2: BHNS merger efficiency for YSCs $\eta_{\rm YSC}$; column 3: BHNS merger efficiency for isolated binaries $\eta_{\rm IB}$, from Giacobbo & Mapelli (2018).

Z	$\eta_{\rm YSC}$ (M$_\odot^{-1}$)	$\eta_{\rm IB}$ (M$_\odot^{-1}$)
0.0002	1.8×10^{-6}	1.7×10^{-5}
0.002	2.1×10^{-6}	2.4×10^{-5}
0.02	1.1×10^{-7}	2.6×10^{-9}

This result can be interpreted as follows. In metal-poor environments, where very massive BHs can form ($m_{\rm BH} \geq 30$ M$_\odot$), exchanges favour the formation of BBHs and suppress the formation of BHNSs, because NSs are much lighter than BHs. In metal-rich environments, where BHs are rather light, dynamics enhances the merger rate of BHNSs.

From the merger efficiency, we can estimate the merger rate density in the local Universe as described in Santoliquido et al. (2020):

$$\mathcal{R}_{\rm BHNS} = \frac{1}{t_{\rm lb}(z_{\rm loc})} \int_{z_{\rm max}}^{z_{\rm loc}} \psi(z') \frac{{\rm d}t_{\rm lb}}{{\rm d}z'} {\rm d}z' \times \int_{Z_{\rm min}(z')}^{Z_{\rm max}(z')} \eta(Z)\, \mathcal{F}(z', z_{\rm loc}, Z)\, {\rm d}Z, \quad (2)$$

where $t_{\rm lb}(z_{\rm loc})$ is the look-back time evaluated in the local universe ($z_{\rm loc} \leq 0.1$), $\psi(z')$ is the cosmic SFR density at redshift z' (from Madau & Fragos 2017), $Z_{\rm min}(z')$ and $Z_{\rm max}(z')$ are the minimum and maximum metallicities of stars formed at redshift z', respectively, and $\mathcal{F}(z', z_{\rm loc}, Z)$ is the fraction of BHNSs that form at redshift z' from stars with metallicity Z and merge at redshift $z_{\rm loc}$ normalized to all BHNSs that form from stars with metallicity Z. To calculate the look-back time $t_{\rm lb}$, we take the cosmological parameters (H_0, $\Omega_{\rm M}$, and Ω_Λ) from Ade et al. (2016). We integrate equation (2) up to redshift $z_{\rm max} = 15$, which we assume to be the epoch of formation of the first stars.

From equation (2), we obtain a local merger rate density $\mathcal{R}_{\rm BHNS} \sim 28$ Gpc^{-3} yr^{-1}, by assuming that all the cosmic star formation rate occurs in YSCs like the ones we simulated in this paper. For the isolated binaries, we find $\mathcal{R}_{\rm BHNS} \sim 49$ Gpc^{-3} yr^{-1} (Santoliquido et al. 2020).

The models presented in this work assume low natal kicks for NSs, which are in tension with the proper motions of some Galactic young pulsars (Giacobbo & Mapelli 2018). We recently proposed a new model for natal kicks (Giacobbo & Mapelli 2020) that can reproduce the proper motions of Galactic pulsars and gives a value for the merger rate close to the one presented in this study for isolated BHNSs. As a result, we do not expect significant differences in the merger rate density between the model adopted in this work and the one proposed by Giacobbo & Mapelli (2020).

3.5 GW190814

While we were addressing the reviewer's comments, the LVC published the discovery of GW190814 (Abbott et al. 2020b), a binary compact object merger with a total mass of $25.8^{+1.0}_{-0.9}$ M$_\odot$ and

a mass ratio of $q = 0.112^{+0.008}_{-0.009}$. GW190814 might be either a BBH or a BHNS, depending on the nature of the secondary component, which has a mass of $m_2 = 2.59^{+0.08}_{-0.09}$ $M_\odot$. In our models, dynamical BHNSs with a total mass of $\sim$26 $M_\odot$ are rather common, while isolated BHNSs with such high total mass and low mass ratio are extremely rare.

In our simulations, we do not have any NS with a mass of >2 $M_\odot$, but this is an effect of our assumptions for the core-collapse SN model: We use the rapid core-collapse SN model by Fryer et al. (2012), which was designed to enforce a mass gap between 2 and 5 $M_\odot$. If we had run our simulations with, e.g. the delayed core-collapse SN model by the same authors, the gap between 2 and 5 $M_\odot$ would have disappeared.

The local merger rate density of GW190814-like systems inferred from the LVC is $\sim 7^{+16}_{-6}$ Gpc^{-3} yr^{-1} (Abbott et al. 2020b). With the method described in Section 3.4, we estimate a local merger rate density of $\sim$0 and $\sim 8^{+4}_{-4}$ Gpc^{-3} yr^{-1} for isolated and dynamical GW190814-like systems, respectively. Here, we define GW190814-like systems as all simulated BHNS mergers with a total mass of 20–30 $M_\odot$.

If we interpret GW190814 as a BBH, rather than a BHNS, we still expect that such extreme mass ratio is rather prohibitive for isolated binary evolution, while it is common in dynamical BBHs (see e.g. the companion papers by Di Carlo et al. 2019b, 2020). Hence, our models strongly support a dynamical formation for GW190814 in a YSC.

4 CONCLUSIONS

We have studied the formation of BHNSs in 100 002 low-mass (300–1000 $M_\odot$) YSCs by means of direct *N*-body simulations coupled with binary population synthesis. We have used a version of NBODY6++GPU (Wang et al. 2015) interfaced with our population-synthesis code MOBSE (Giacobbo et al. 2018), as described in Di Carlo et al. (2019b). Very few studies address the dynamics of BHNSs (Devecchi et al. 2007; Clausen et al. 2013; Fragione & Loeb 2019a,b; Ye et al. 2020) and none of them focus on YSCs. YSCs are generally less massive than globular clusters and short lived, but they form all the time across cosmic history: YSCs are the main nursery of stars in the local Universe. Moreover, none of the previous works investigate the impact of star cluster dynamics on the mass of BHNSs.

We find that BHNSs formed in YSCs are significantly more massive than BHNSs formed from isolated binary evolution. At low metallicity, the mass of the BH component in a BHNS can reach $\sim$160 $M_\odot$ in YSCs and $\sim$65 $M_\odot$ in isolated binaries. If we focus on dynamical BHNSs that merge within a Hubble time by GW emission, the vast majority of BHNSs in isolated binaries ($>$99 per cent) have masses of $m_{\rm BHNS} \leq 15$ $M_\odot$, while $\sim$40 per cent of BHNSs in YSCs have masses of $m_{\rm BHNS} > 15$ $M_\odot$. The mass range of dynamical BHNSs in our models strongly supports a dynamical formation for GW190814 (Abbott et al. 2020b). Interestingly, not only the exchanged BHNSs (i.e. BHNS systems formed by dynamical exchanges) but also original BHNSs in YSCs (i.e. BHNS systems that form in a YSC from the evolution of a primordial binary star) are significantly more massive than BHNSs formed in isolation. This indicates that dynamical hardening is important for BHNSs in YSCs.

Our simulations do not include compact object spins, because of the large theoretical uncertainties about their magnitude. On the other hand, we expect that dynamical encounters completely randomize the direction of the spins, at least in the case of exchanged binaries (Bouffanais et al. 2019). This implies that our dynamical BHNSs have non-zero components of the spin in the orbital plane, showing precession. Binaries with non-aligned spins and small mass ratio $q_{\rm BHNS} = m_{\rm NS}/m_{\rm BH}$ are not expected to be accompanied by bright electromagnetic counterparts (e.g. Zappa et al. 2019).

All the BHNSs formed in YSCs merge after they were ejected from their parent star cluster. This implies that a large fraction of BHNS mergers in the field might have formed in YSCs.

In metal-poor YSCs ($Z = 0.0002$ and 0.002), the BHNS merger efficiency of YSCs is a factor of 10 lower than that of isolated binaries. In contrast, at solar metallicity ($Z = 0.02$) the BHNS merger efficiency of YSCs is a factor of 40 higher than the BHNS merger efficiency of isolated binaries: Dynamics triggers a significant number of BHNS mergers at solar metallicity and reduces the differences between metal-poor and metal-rich environments.

Finally, we estimate a local merger rate density of $\mathcal{R}_{\rm BHNS} \sim 28$ Gpc^{-3} yr^{-1}, similar to recent estimates from isolated binary evolution (Mapelli & Giacobbo 2018; Artale et al. 2019; Baibhav et al. 2019; Giacobbo & Mapelli 2020; Santoliquido et al. 2020; Tang et al. 2020) and below the upper limit inferred from the first and second observing runs of LIGO and Virgo (Abbott et al. 2019). Hence, a large fraction of BHNS mergers occurring in the field might have originated in a YSC. We expect that the mass spectrum of BHNS mergers from GW detections will provide a clue to differentiate between dynamical and isolated formation of BHNSs.

ACKNOWLEDGEMENTS

We thank the referee, Dr. Mirek Giersz, for his useful comments, which helped us improving this work. MM, AB, GI, NG, and SR acknowledge financial support by the European Research Council for the ERC Consolidator grant DEMOBLACK, under contract no. 770017. MS acknowledges funding from the European Union's Horizon 2020 research and innovation programme under the Marie-Sklodowska-Curie grant agreement no. 794393. UNDC acknowledges financial support from Università degli Studi dell'Insubria through a Cycle 33rd PhD grant. We thank G. Costa and M. Pasquato for interesting and stimulating discussion. We are grateful to L. Wang for his helpful support on NBODY6++GPU. All the *N*-body simulations discussed in this paper were performed with the supercomputer DEMOBLACK at the Physics and Astronomy department 'G. Galilei' of the University of Padova, equipped with 192 cores and 8 NVIDIA Tesla V100 GPUs.

DATA AVAILABILITY

The data underlying this article will be shared on reasonable request to the corresponding authors.

REFERENCES

Aarseth S. J., 2012, MNRAS, 422, 841
Abbott B. P. et al., 2016a, Phys. Rev. X, 6, 041015
Abbott B. P. et al., 2016b, Phys. Rev. Lett., 116, 061102
Abbott B. P. et al., 2016c, Phys. Rev. Lett., 116, 241103
Abbott B. P. et al., 2017a, Phys. Rev. Lett., 118, 221101
Abbott B. P. et al., 2017b, Phys. Rev. Lett., 119, 141101
Abbott B. P. et al., 2017c, ApJ, 851, L35
Abbott B. P. et al., 2019, Phys. Rev. X, 9, 031040
Abbott B. P. et al., 2020a, ApJ, 892, L3
Abbott B. P. et al., 2020b, ApJ, 896, L44
Ade P. A. R., Aghanim N., Arnaud M., Lähteenmäki A., Lamarre J. M., Lasenby A., Lattanzi M., 2016, A&A, 594, A13
Andreoni I. et al., 2020, ApJ, 890, 131
Arca Sedda M., Mastrobuono-Battisti A., 2019, preprint (arXiv:1906.05864)

Artale M. C., Mapelli M., Giacobbo N., Sabha N. B., Spera M., Santoliquido F., Bressan A., 2019, MNRAS, 487, 1675
Baibhav V., Berti E., Gerosa D., Mapelli M., Giacobbo N., Bouffanais Y., Di Carlo U. N., 2019, Phys. Rev. D, 100, 064060
Ballone A., Mapelli M., Di Carlo U. N., Torniamenti S., Spera M., Rastello S., 2020, MNRAS, 496, 49
Banerjee S., 2017, MNRAS, 467, 524
Banerjee S., 2018, MNRAS, 473, 909
Banerjee S., Baumgardt H., Kroupa P., 2010, MNRAS, 402, 371
Banerjee S., Belczynski K., Fryer C. L., Berczik P., Hurley J. R., Spurzem R., Wang L., 2019, preprint (arXiv:1902.07718)
Barbieri C., Salafia O. S., Colpi M., Ghirlanda G., Perego A., Colombo A., 2019, ApJ, 887, L35
Belczynski K., Taam R. E., Kalogera V., Rasio F. A., Bulik T., 2007, ApJ, 662, 504
Belczynski K., Bulik T., Fryer C. L., Ruiter A., Valsecchi F., Vink J. S., Hurley J. R., 2010, ApJ, 714, 1217
Bethe H. A., Brown G. E., 1998, ApJ, 506, 780
Bethe H. A., Brown G. E., 1999, ApJ, 517, 318
Blinnikov S. I., Novikov I. D., Perevodchikova T. V., Polnarev A. G., 1984, Sov. Astron. Lett., 10, 177
Bouffanais Y., Mapelli M., Gerosa D., Di Carlo U. N., Giacobbo N., Berti E., Baibhav V., 2019, ApJ, 886, 25
Choksi N., Volonteri M., Colpi M., Gnedin O. Y., Li H., 2019, ApJ, 873, 100
Clausen D., Sigurdsson S., Chernoff D. F., 2013, MNRAS, 428, 3618
Clausen D., Sigurdsson S., Chernoff D. F., 2014, MNRAS, 442, 207
Devecchi B., Colpi M., Mapelli M., Possenti A., 2007, MNRAS, 380, 691
Di Carlo U. N., Mapelli M., Bouffanais Y., Giacobbo N., Santoliquido F., Bressan S., Spera M., Haardt F., 2019a, preprint (arXiv:1911.01434)
Di Carlo U. N., Giacobbo N., Mapelli M., Pasquato M., Spera M., Wang L., Haardt F., 2019b, MNRAS, 487, 2947
Di Carlo U. N. et al., 2020, MNRAS, 497, 1043
Dominik M. et al., 2015, ApJ, 806, 263
Eichler D., Livio M., Piran T., Schramm D. N., 1989, Nature, 340, 126
Farrow N., Zhu X.-J., Thrane E., 2019, ApJ, 876, 18
Fernández R., Foucart F., Kasen D., Lippuner J., Desai D., Roberts L. F., 2017, Class. Quantum Gravity, 34, 154001
Fragione G., Kocsis B., 2018, Phys. Rev. Lett., 121, 161103
Fragione G., Loeb A., 2019a, MNRAS, 486, 4443
Fragione G., Loeb A., 2019b, MNRAS, 490, 4991
Fragos T., Andrews J. J., Ramirez-Ruiz E., Meynet G., Kalogera V., Taam R. E., Zezas A., 2019, ApJ, 883, L45
Fryer C. L., Woosley S. E., Hartmann D. H., 1999, ApJ, 526, 152
Fryer C. L., Belczynski K., Wiktorowicz G., Dominik M., Kalogera V., Holz D. E., 2012, ApJ, 749, 91
Fujii M. S., Tanikawa A., Makino J., 2017, PASJ, 69, 94
Giacobbo N., Mapelli M., 2018, MNRAS, 480, 2011
Giacobbo N., Mapelli M., 2019, MNRAS, 482, 2234
Giacobbo N., Mapelli M., 2020, ApJ, 891, 141
Giacobbo N., Mapelli M., Spera M., 2018, MNRAS, 474, 2959
Goodwin S. P., Whitworth A. P., 2004, A&A, 413, 929
Heggie D. C., 1975, MNRAS, 173, 729
Hills J. G., Fullerton L. W., 1980, AJ, 85, 1281
Hong J., Vesperini E., Askar A., Giersz M., Szkudlarek M., Bulik T., 2018, MNRAS, 480, 5645
Hurley J. R., Tout C. A., Pols O. R., 2002, MNRAS, 329, 897
Kremer K., Ye C. S., Chatterjee S., Rodriguez C. L., Rasio F. A., 2020 , in Bragaglia A., Davies M., Sills A., Vesperini E., eds, Proc. IAU Symp. 351, Star Clusters: From the Milky Way to the Early Universe. Kluwer, Dordrecht, p. 357
Kroupa P., 2001, MNRAS, 322, 231
Kuhn M. A., Hillenbrand L. A., Sills A., Feigelson E. D., Getman K. V., 2019, ApJ, 870, 32
Kumamoto J., Fujii M. S., Tanikawa A., 2019, MNRAS, 486, 3942
Kumamoto J., Fujii M. S., Tanikawa A., 2020, MNRAS, 495, 4268
Küpper A. H. W., Maschberger T., Kroupa P., Baumgardt H., 2011, MNRAS, 417, 2300
Lada C. J., Lada E. A., 2003, ARA&A, 41, 57
Madau P., Fragos T., 2017, ApJ, 840, 39
Mao S., Narayan R., Piran T., 1994, ApJ, 420, 171
Mapelli M., 2016, MNRAS, 459, 3432
Mapelli M., Bressan A., 2013, MNRAS, 430, 3120
Mapelli M., Giacobbo N., 2018, MNRAS, 479, 4391
Mapelli M., Giacobbo N., Ripamonti E., Spera M., 2017, MNRAS, 472, 2422
Mapelli M., Giacobbo N., Santoliquido F., Artale M. C., 2019, MNRAS, 487, 2
Mapelli M., Spera M., Montanari E., Limongi M., Chieffi A., Giacobbo N., Bressan A., Bouffanais Y., 2020, ApJ, 888, 76
Marks M., Kroupa P., Dabringhausen J., Pawlowski M. S., 2012, MNRAS, 422, 2246
Moe M., Di Stefano R., 2015, ApJ, 810, 61
Narayan R., Piran T., Shemi A., 1991, ApJ, 379, L17
O'Shaughnessy R., Kalogera V., Belczynski K., 2010, ApJ, 716, 615
Özel F., Freire P., 2016, ARA&A, 54, 401
Paczynski B., 1991, Acta Astron., 41, 257
Peters P. C., 1964, Phys. Rev., 136, 1224
Pfahl E., Podsiadlowski P., Rappaport S., 2005, ApJ, 628, 343
Popham R., Woosley S. E., Fryer C., 1999, ApJ, 518, 356
Portegies Zwart S. F., McMillan S. L. W., 2000, ApJ, 528, L17
Portegies Zwart S. F., Baumgardt H., Hut P., Makino J., McMillan S. L. W., 2004, Nature, 428, 724
Portegies Zwart S. F., McMillan S. L. W., Gieles M., 2010, ARA&A, 48, 431
Rastello S., Amaro-Seoane P., Arca-Sedda M., Capuzzo-Dolcetta R., Fragione G., Tosta e Melo I., 2019, MNRAS, 483, 1233
Rodriguez C. L., Morscher M., Pattabiraman B., Chatterjee S., Haster C.-J., Rasio F. A., 2015, Phys. Rev. Lett., 115, 051101
Rodriguez C. L., Chatterjee S., Rasio F. A., 2016, Phys. Rev. D, 93, 084029
Rodriguez C. L., Amaro-Seoane P., Chatterjee S., Kremer K., Rasio F. A., Samsing J., Ye C. S., Zevin M., 2018, Phys. Rev. D, 98, 123005
Rodriguez C. L., Zevin M., Amaro-Seoane P., Chatterjee S., Kremer K., Rasio F. A., Ye C. S., 2019, Phys. Rev. D, 100, 043027
Ruffert M., Janka H. T., 1999, A&A, 344, 573
Samsing J., 2018, Phys. Rev. D, 97, 103014
Samsing J., Hamers A. S., Tyles J. G., 2019, Phys. Rev. D, 100, 043010
Sana H. et al., 2012, Science, 337, 444
Sánchez N., Alfaro E. J., 2009, ApJ, 696, 2086
Santoliquido F., Mapelli M., Bouffanais Y., Giacobbo N., Di Carlo U. N., Rastello S., Artale M. C., Ballone A., 2020, preprint (arXiv:2004.09533)
Sigurdsson S., Hernquist L., 1993, Nature, 364, 423
Sigurdsson S., Phinney E. S., 1995, ApJS, 99, 609
Sipior M. S., Sigurdsson S., 2002, ApJ, 572, 962
Spera M., Mapelli M., 2017, MNRAS, 470, 4739
Spera M., Mapelli M., Giacobbo N., Trani A. A., Bressan A., Costa G., 2019, MNRAS, 485, 889
Spitzer L., 1987, Dynamical Evolution of Globular Clusters. Princeton Univ. Press, Princeton, NJ
Tang P. N., Eldridge J. J., Stanway E. R., Bray J. C., 2020, MNRAS, 493, L6
Tanikawa A., 2013, MNRAS, 435, 1358
Tauris T. M. et al., 2017, ApJ, 846, 170
Wang L., Spurzem R., Aarseth S., Nitadori K., Berczik P., Kouwenhoven M. B. N., Naab T., 2015, MNRAS, 450, 4070
Wang L. et al., 2016, MNRAS, 458, 1450
Wei H., Feng M., 2019, preprint (arXiv:1912.03466)
Weidner C., Kroupa P., 2006, MNRAS, 365, 1333
Weidner C., Kroupa P., Bonnell I. A. D., 2010, MNRAS, 401, 275
Ye C. S., Fong W.-f., Kremer K., Rodriguez C. L., Chatterjee S., Fragione G., Rasio F. A., 2020, ApJ, 888, L10
Zappa F., Bernuzzi S., Pannarale F., Mapelli M., Giacobbo N., 2019, Phys. Rev. Lett., 123, 041102
Ziosi B. M., Mapelli M., Branchesi M., Tormen G., 2014, MNRAS, 441, 3703

This paper has been typeset from a TEX/LATEX file prepared by the author.